Minerals Engineering 246 (2026) 110400

Contents lists available at ScienceDirect

Minerals Engineering

journal homepage: www.elsevier.com/locate/mineng

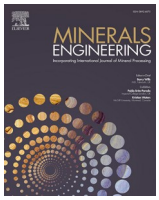

Opto-magnetic sorting via water-based wetting and magnetic lifting for coarse REE ore pre-concentration

Hongli Su *, Alim Yolalmaz, Rajeev Bheemireddy, Yongli Wu *, Peter Rem, Francesco Di Maio *

Resource & Recycling, Department of Engineering Structures, Faculty of Civil Engineering and Geosciences, Delft University of Technology, Delft 2628, CN, the Netherlands

ARTICLE INFO

Keywords:
Rare earth elements
Opto-magnetic sorting
Coarse particle separation
Pre-concentration
Sensor-based sorting

ABSTRACT

Mineral grinding often represents a major fraction of total energy costs and coarse pre-concentration can significantly decrease unnecessary processing of barren material. Compressed-air ejection is effective at industrial scale, but suffers from low accuracy at millimeter scale. An opto-magnetic sorting process for coarse pre-concentration of REE-bearing particles before grinding was developed and assessed at labscale. The process combines image-based optical thresholding, water-based wetting of selected particles, magnetite adhesion to wetted surfaces, and magnetic lifting. This process thus couples selective magnetite coating (enabled by localized wetting) and magnetic lifting for particle sorting. The process was run in a reject-oriented mode to facilitate early mass rejection before subsequent comminution. Lab-scale experiments on rauhaugite revealed increasing pre-concentration with decreasing particle size, resulting in a low-grade fraction of 30.4 wt% of the 2–4 mm feed for possible early rejection. The high-grade fraction (57% of the 2–4 mm feed) achieved a TREO concentration of 2.32%, reflecting an enrichment factor of approximately 1.35 compared to the feed (1.71%), consistent with a partial realization of the intrinsic upgrading potential of the ore at this mass yield, as inferred from the TREO distribution of RGB-classified particles. The lab system processed 84 kg/h, corresponding to approximately 1 tonne of feed processed within 12 h. Based on an instantaneous power demand of ~ 0.8 kW, this corresponds to an energy consumption of ~ 9.6 kWh/tonne under steady-state conditions. The process also exhibited low water usage (~5.7 L/tonne feed) and > 99% magnetite recyclability (after 3 runs). Beyond REE beneficiation, the proposed approach shows potential for selective pre-concentration of heterogeneous particulate streams requiring localized actuation.

1. Introduction

Rare earth elements (REEs) are strategically important mineral resources (Cuadros-Muñoz, 2024; Balaram, 2019; Opare et al., 2021; Zhou et al., 2017) and widely used in advanced materials and technologies (e.g., catalysts, magnets, phosphors) (Ghorbani, 2025; Tanabe, 2015; Du, 2025; Lebrouhi, 2022; Bai, 2024; Supriya, 2023; Tan et al., 2017; Zhao, 2025). However, beneficiation of REE ores is energy-intensive, with comminution accounting for a significant portion of operational cost and energy consumption (Norgate and Haque, 2010; Tromans, 2008). Due to the typically low grade of primary REE ores, a substantial fraction of processed material ultimately reports to tailings (Chen, 2020). Thus, early-stage mass rejection is critical to reduce downstream comminution demand (Peukert et al., 2022). Coarse particle pre-concentration has emerged as an effective approach to reject low-grade materials entering downstream and improve overall separation efficiency (Sala-Garrido, 2024; Wübbeke, 2013; Nadolski, 2018). By selectively removing low-grade particles before comminution, pre-concentration can decrease unnecessary processing of barren material, enhance the efficiency of subsequent beneficiation stages, and result in lower energy demand (Qiu and Wang, 2019).

Sensor-based ore sorting has emerged as a promising approach for coarse particle separation (Peukert et al., 2022; Modise, 2022; Wotruba and Robben, 2020). Conventional industrial systems usually involve compressed air ejection or mechanical deflection. These methods are effective at high throughput. Nevertheless, there are challenges in highly localized particle actuation (or lifting) at the millimeter scale. This is because of airflow dispersion, unintended movement of

* Corresponding authors.
E-mail addresses: H.Su-3@tudelft.nl (H. Su), Y.Wu-7@tudelft.nl (Y. Wu), F.DiMaio@tudelft.nl (F. Di Maio).

https://doi.org/10.1016/j.mineng.2026.110400
Received 26 February 2026; Received in revised form 7 May 2026; Accepted 14 May 2026
Available online 16 May 2026

neighboring particles, and the demand for compressed airflow. These limitations are especially significant when dealing with ores showing little liberation at particle sizes in the range suitable for compressed air ejection, such as heterogeneous REE-bearing particles that are categorized as coarse to mid-size. Water coating and magnetic lifting strategies for REE pre-concentration attract interest for their intrinsic power to eject efficiently at millimeter scale, but systematic experimental validation is still limited.

Using 2–4 mm rauhaugite, we designed and developed an opto-magnetic assisted sorter, which combines optical detection, selective water wetting, magnetite deposition, and magnetic lifting under a low-intensity magnetic field (Fig. 1A) to reject low-grade particles before grinding (Peukert et al., 2022). The process converts image-based particle classification into a physical separation response: optically selected particles are locally wetted with water, coated with magnetite powder, and subsequently lifted under a magnetic field, bypassing the need for compressed-air ejection. Ore-specific RGB thresholding is employed as a controllable, low-latency method to validate the detection concept under real-time imaging conditions. The system was evaluated using grade, recovery, yield/mass distribution, throughput, and resource-use indicators. This sorter rejected 30.4 wt% of the feed before grinding, upgrading the remaining stream in a subsequent step to 2.32 wt% total rare earth oxide (TREO) at 57 wt% yield.

2. Materials and methods

2.1. Materials and chemicals

Deionized (DI) water with a resistivity of ~1.6 MΩ/cm was prepared by a Milli-Q ultrapure water purification system (Merck) for selective surface wetting. Magnetite powder (magnetite, Fe_3O_4 98%, fine magnetite powder, density ~ 5.1 t/m^3) was purchased from LKAB (Sweden) as a reusable magnetic carrier material. Its particle size distribution is shown in Fig. 2. The relatively fine particle size distribution facilitates stable adhesion onto selectively wetted particle surfaces and supports subsequent magnetic lifting. Rauhaugite ores were provided by Saga Rare Earths AS (Norway) and used as representative REE-bearing ores for evaluating the feasibility of optical pre-concentration.

2.2. Preparation of materials

The rauhaugite ores were crushed by a jaw crusher (Retsch, model, Germany) and sieved by a sieve shaker (NEXOPART, model, Germany) at TU Delft, Netherlands, to select 2–4 mm particles for sorting. Particle size selection was guided by the expected trade-off between throughput and achievable enrichment in coarse pre-concentration, with smaller particles favouring improved optical discrimination, wetting, and magnetite-assisted lifting. Following sorting, the collected particle fractions were milled to a homogeneous fine powder (~100 μm) using a Retsch PM100 planetary ball mill before elemental analysis.

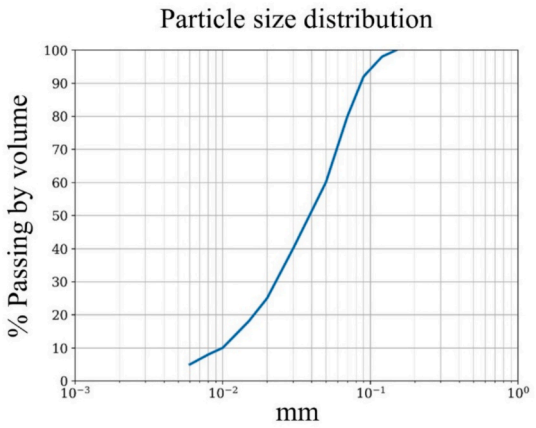

Fig. 2. Particle size distribution of magnetite powder (provided by LKAB, Sweden).

2.3. Characterization

The REE elements were identified using laser-induced breakdown spectroscopy (LIBS; Keyence, EA-300, Belgium). The REE concentrations were characterized by x-ray fluorescence spectroscopy (XRF, Evident Scientific, Vanta Max, Japan) and inductively coupled plasma mass spectrometry (ICP-MS, Agilent Technologies, 7700 series, United States). ICP measurements were used as the reference for the final TREO grade values reported in this study. Individual REE concentrations were converted to their corresponding oxides (REO), and TREO content was calculated as the sum of all measured REO components. TREO recovery and grade were used as primary indicators for evaluating sorting performance.

2.4. Workflow

The workflow consists of four coupled steps: particle-size preparation, optical detection, selective surface functionalization, and magnetic lifting/separation (Fig. 1B). First, raw ores are crushed and screened to obtain a suitable size fraction for opto-magnetic sorting. The particles are then conveyed through the detection zone, where images are acquired and transmitted to the workstation for real time classification. Particle selection is based on the RGB (red, green, and blue) intensity characteristics (Fig. 3). A constant pixel-level threshold value has been set in the red channel throughout the experiments. The threshold value has been determined based on a training set of data collected under the same imaging conditions. Imaging conditions (illumination, camera geometry and white balance) are kept constant across runs, and flat-field correction with a white reference is applied before red-channel thresholding. Pixel-threshold detection is used to satisfy the belt-synchronization latency budget for real-time lifting; particle segmentation is feasible but not expected to materially change the reported stream-level metrics under the present conditions. Under the present imaging conditions, actuation depended on optically distinct surface

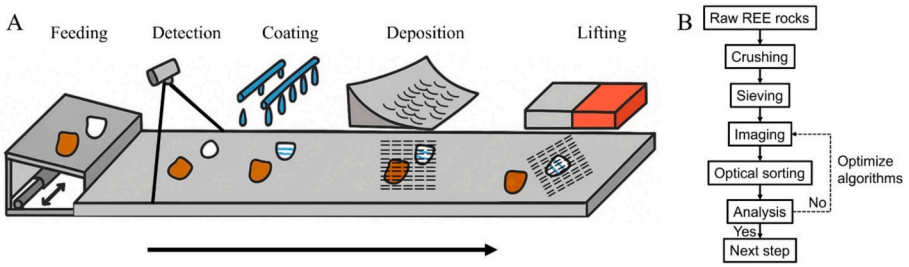

Fig. 1. (A) Principle of the opto-magnetic assisted sorter. (B) The whole workflow for pre-concentration of REEs, including opto-magnetic sorting.

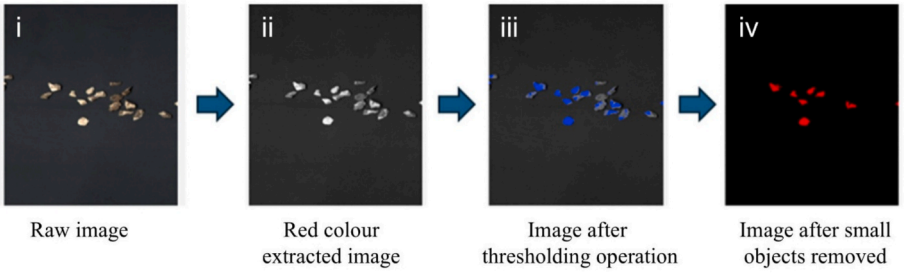

Fig. 3. Image processing steps.

regions rather than precise particle boundaries. Pixel-threshold detection was therefore considered sufficient for the present study.

After optical identification, a thin water film was selectively deposited onto the target particles to promote controlled magnetite attachment and thereby render them magnetically liftable. With the magnetite dosage kept constant, the water volume per pixel (5–20 pL) was adjusted to balance lifting stability, selectivity, and water consumption. The magnetite-coated particles were then exposed to magnetic lifting, whereas non-wetted particles did not acquire sufficient magnetite and therefore were not lifted. Thus, optical classification was translated into a differential magnetic response and subsequently into physical separation. A low-intensity magnet (0.11 T) integrated into the roller magnetic sorter was used to separate lifted mineral particles from the attached magnetite powder (Fig. 4). Owing to their higher mass, the mineral particles detached more readily from the magnetic field and fell into the target particle container, whereas the lighter magnetite powder remained magnetically responsive for longer, was carried further, and was subsequently recovered by the upper belt magnetic separator. Feeding, detection, classification, and lifting were fully automated. The as-obtained particles are collected separately and ball-milled into fine powder for chemical analysis. Sorting performance was evaluated using enrichment, energy consumption, water usage, magnetite reuse, and throughput. When enrichment was insufficient, the sorting conditions (e.g., threshold color intensity in red channel) were adjusted iteratively based on the analytical results.

2.5. Sorting system operating parameters

The key experimental and operating conditions used in the present study are summarized in Table 1.

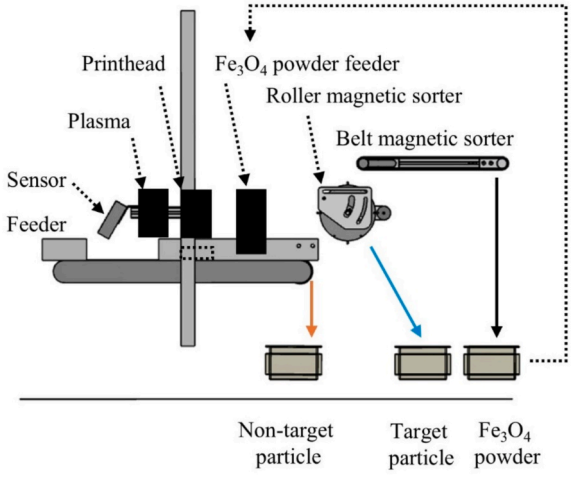

Fig. 4. Separation route of mineral particles and magnetite powder in the magnetic lifting unit.

Table 1
Experimental parameters.

Group	Parameter	Value	Unit
Feed & objective	Ore type	Rauhaugite	
	Primary size fraction	2–4	mm
	Mass	200	g
Detection & actuation	Detection method	Pixel-based thresholding	
	Classification feature	Red-channel threshold	
	Actuation mechanism	Selective wetting + magnetic lifting	
	Wetting fluid	DI water	
	DI water resistivity	~1.6	MΩ·cm
	Droplet volume (selected)	15	pL
Operating & resources	Belt speed (test)	0.1	m/s
	Magnetite material density	~5.1 (supplier data)	t/m^3
	Practical operating magnetic field (permanent magnet)*	0.11	T
	Throughput (lab setup)	84	kg/h
	Process 1 tonne feed	~12	h
	Power draw (lab setup)	~9.6	kWh/ tonne feed
	Total water usage	5.7	L/tonne feed
	Magnetite consumption per run	<1.2	kg/tonne feed
	Magnetite recyclability (after 3 runs)	>99	%

* A permanent magnet providing a field strength of 0.11 T was used in the current prototype. This value was selected as a practical operating condition for concept validation to ensure stable lifting after selective wetting and magnetite adhesion, rather than as a globally optimized magnetic field.

2.6. Data quality and repeatability

Each separation condition was tested in triplicate (n = 3), and results are reported as mean ± SD. Triplicates are defined as self-contained sorting runs, encompassing feeding, detection, lifting, fraction collection, and downstream chemical analysis. Given the exploratory lab-scale scope and the small sample size, the data are presented descriptively without inferential statistical testing. This study was intended as a concept-level feasibility assessment under controlled lab conditions, focusing on whether synchronized detection, selective wetting, magnetite adhesion, magnetic lifting, and stream-level fractionation could be achieved repeatedly in the current prototype. The results should not be interpreted as statistical confirmation of process robustness. Broader statistical validation across larger datasets and more variable operating conditions remains future work. Mass yield was determined from the measured mass of the recovered fractions relative to the feed mass.

TREO grade and recovery were determined from XRF/ICP analysis as specified in Table 2. Mass and TREO balance calculations were conducted between the feed and all recovered product fractions (1A-1C) to ensure internal consistency of the sorting performance data. The current process was operated in a reject-oriented mode, in which low-grade particles were selected for wetting and subsequent magnetic lifting. This involved the removal of fraction 1A, followed by fraction 1B in the second step, while the rest of the particles were collected as fraction 1C (high-grade fraction).

3. Results and discussion

3.1. Selective surface functionalization and energy-efficient lifting

3.1.1. Water-based selection vs air-based lifting

Selective surface functionalization is an important step in the proposed sorting method, as it directly impacts the selectivity of the subsequent magnetic lifting steps and the auxiliary resource consumption. For the surface functionalization method used in this study, a selective wetting/coating step is used as a method to functionalize water-coated particles prior to magnetic lifting.

Air-jet systems rely on a short burst of compressed air to blow the target particles into a certain collector, allowing high-throughput sorting at the industrial level (Robben and Wotruba, 2019; Salter and Wyatt, 1991). However, airflow distribution and secondary displacement of other particles may decrease selectivity by the air-jet systems for millimeter-scale particles. Water deposition is capable of picoliter-scale droplet deposition to selectively targeted regions of particles without direct mechanical displacement, which allows for localized surface modification for subsequent magnetite adhesion and magnetic lifting. This study focuses on millimeter-scale particle separation, the water-based method had sufficient locality to achieve efficient and effective sorting.

3.1.2. Coating liquid selection

Candidate jetting fluids were screened based on three practical criteria: (i) jetting stability at the selected belt speeds, (ii) ability to generate localized wetting on target particles, and (iii) material cost for potential scale-up use. Liquid selection was guided by the need to balance functional performance and economic viability. The most used liquid in inkjet systems is Siegwerk Flush due to its stable jetting behavior. However, its high price (~15 €/L) and limited recyclability significantly limit its broader application. Alternative fluids such as Dowanol TPM, DI water, and Dowanol-DI water mixtures were therefore investigated as low-cost options. A comparative cost analysis (Fig. 5A) highlights the economic advantages of these alternatives over commercial flush fluids. Dropwatcher observations showed that both DI water and Dowanol TPM could be jetted under the tested conditions. At higher droplet frequency, reduced droplet spacing and the occasional formation of satellite droplets were observed (Fig. 5B), indicating a decrease in jetting stability. Despite this, DI water provided sufficiently stable droplet formation and accurate placement under the selected operating conditions, while avoiding the additional cost and handling requirements associated with organic solvents. Because the purpose of this step is only to create temporary localized wetting for magnetite adhesion, DI water was selected as the coating fluid for subsequent sorting tests.

Table 2
Performance metrics and calculation equations.

Metric	Symbol	Equation	Unit
Mass yield of fraction *i*	Y_i	$Y_i = m_i/m_f \times 100$	%
TREO grade of fraction *i*	G_i		wt%
Feed TREO grade	G_f		wt%
TREO recovery to fraction *i*	R_i	$R_i = m_i G_i / m_f G_f \times 100$	%
Enrichment factor (fraction *i*)	EF_i	$EF_i = G_i/G_f$	
Low-grade mass rejection	MR_{LG}	$MR_{LG} = m_{LG}/m_f \times 100$	%
Water consumption rate	W_r		mL/h
Magnetite recyclability	η_m	$\eta_m = m_{m,recovered}/m_{m,used} \times 100$	%

3.1.3. Water volume

Selectivity and operational reliability can be balanced by the amount of water dropped onto target particles. The volume of water had a significant impact on the stability and selectivity of magnetic lifting. Various volumes of applied water were evaluated to obtain an effective particle surface wetting during the sorting process. The maximum spray volume of the employed water-jetter is 20 pL (Wijshoff, 2010). At a volume of 5 pL, a belt speed of 0.1 m/s and a frenquency of 1,417 Hz, there was insufficient wetting, leading to poor adhesion of magnetite, resulting in frequent failed lifting events (target particles detected but not reliably lifted). At a volume of 20 pL, excessive wetting and misting increased lateral spreading, and neighboring particles were occasionally co-actuated, leading to false extraction (Zhang, 2022). In comparison with 15 pL, at 10 pL there were 30% ± 3% fewer target particles separated correctly (mean ± SD, n = 3), suggesting insufficient wetting for stable magnetite adhesion. Of the conditions tested, the intermediate volume of 15 pL provided the optimal balance of wetting, adhesion stability, and selectivity.

3.2. Opto-magnetic sorting performance and implications for pre-concentration

3.2.1. Sorting response and process meaning (2–4 mm)

Opto-magnetic sorting performance indicates that image-based thresholding can be used to distinguish particles based on different REE content (Fig. 6). Rauhaugite particles (200 g, 2–4 mm) were classified by red-channel intensity thresholds. The threshold refers to the image-classification parameter derived from the red-channel intensity, where lower threshold values correspond to particles with a stronger reddish appearance. LIBS (Fig. 6A), XRF (Table 3), and ICP (Fig. 6C) consistently showed a correlation between surface coloration and REE concentrations. This result suggests that the optical threshold captured mineralogical heterogeneity associated with REE distribution under the present imaging conditions. Thus, ore-specific optical contrast could be translated into physical separation through the subsequent wetting and magnetic lifting steps. The darkest red fraction (1C) accounted for ~ 77.2% of the total TREO and exhibited an increase in TREO grade from ~ 0.81% (1A) to ~ 2.32% (1C), corresponding to ~ 2.85 × enrichment relative to 1A and ~ 1.35 × relative to the feed (Fig. 6D). These results support the use of ore-specific optical appearance as a practical proxy for particle-scale REE distribution in this system. A mass-balance check across feed and products (1A-1C) showed satisfactory closure for both mass and TREO within analytical precision, supporting the reported mass yield, grade, and recovery values (Table 3). The relative analytical characterization (ICP) is shown in Table 4. The ICP results consistently demonstrate increasing concentrations of major REEs (La, Ce, Nd, and Pr) from fraction 1A to 1C, further supporting the correlation between optical response and REE distribution under the present imaging conditions.

The moderate enrichment factor is consistent with the coarse-particle, reject-oriented objective of the process. At this stage, selective rejection of low-grade material (30.4%) is prioritized over maximizing final product grade, and some compositional heterogeneity is expected to remain within each coarse fraction. This is in line with the goal of this unit operation as an upstream pre-concentration operation, in which mass rejection is more important than upgrading.

3.2.2. Process-level implications (illustrative energy/carbon scenario)

To illustrate what early rejection could mean for comminution energy, a simplified mass-balance case was considered with literature values for comminution energy intensity (20–30 kWh per tonne) (Tosun and Konak, 2015). and electricity-related CO_2 emissions (0.3–0.7 kg CO_2

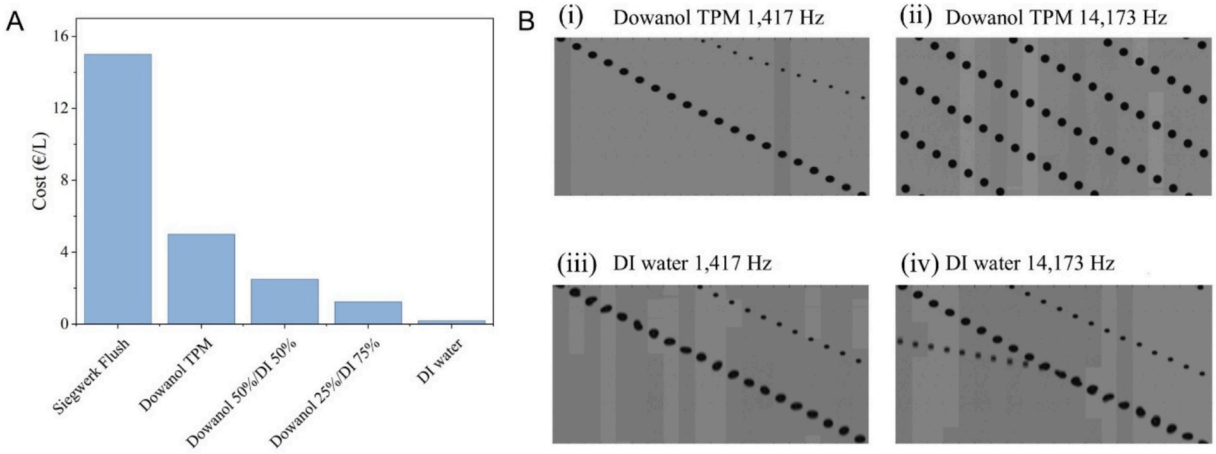

Fig. 5. (A) Comparative cost analysis of jetting fluids. (B) Dropwatcher images of jetting performance for different fluids. Dowanol TPM at droplet frequencies of 1,417 Hz (i) and 14,173 Hz (ii). Deionized water at droplet frequencies of 1,417 Hz (iii) and 14,173 Hz (iv).

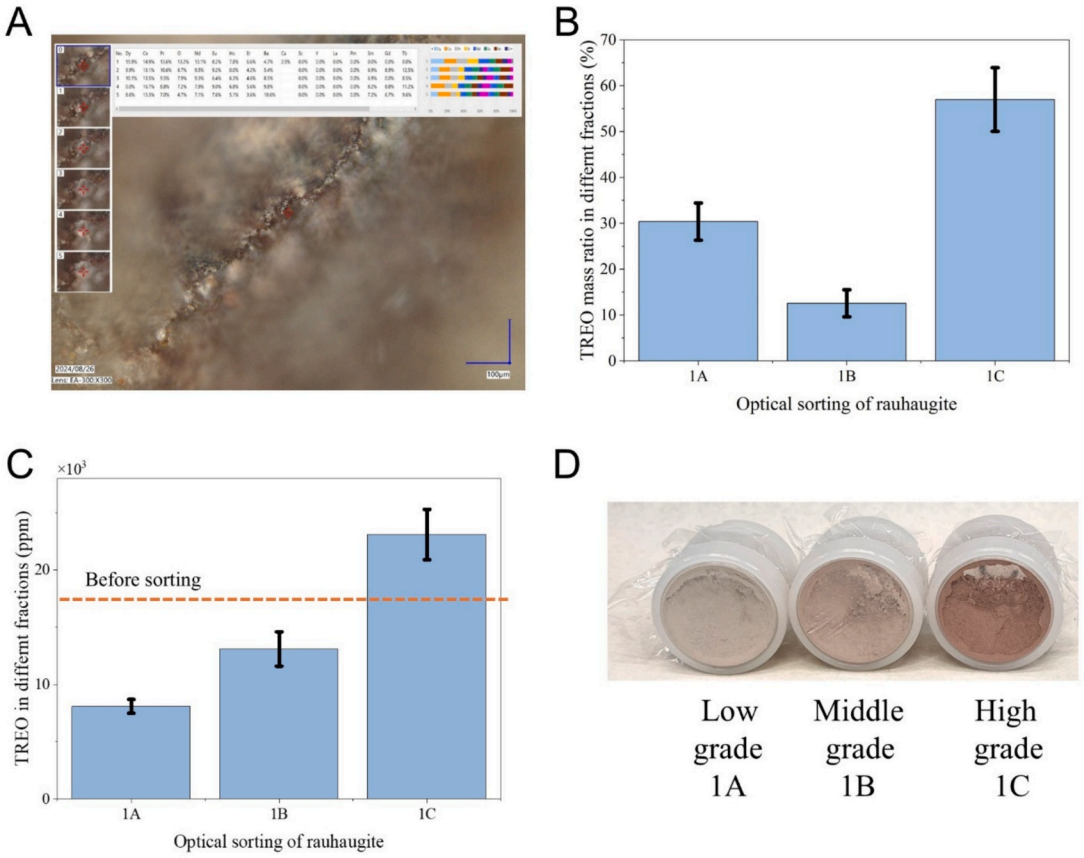

Fig. 6. Optical classification and compositional analysis of rauhaugite particles. (A) LIBS, (B) Mass distribution, (C) TREO concentrations characterized by ICP-MS, illustrating the correlation between surface optical characteristics and REE distribution. Error bars represent standard deviation (n = 3 independent runs), (D) Optical fractions defined by red-channel intensity. (For interpretation of the references to colour in this figure legend, the reader is referred to the web version of this article.)

per kWh) (Braeuer et al., 2020). The comminution energy saving per tonne of feed was estimated as:

$$\Delta E = MR_{LG} \times E_{comminution} \quad (1)$$

where MR_{LG} is the low-grade reject mass fraction and $E_{comminution}$ is the assumed specific comminution energy demand. Based on the measured reject fraction (~30.4%), the illustrative energy saving is $\Delta E \approx 6$–9 kWh per tonne feed. The corresponding CO_2 reduction associated with avoided downstream comminution energy was estimated as:

$$\Delta CO_2 = \Delta E \times EF_{\text{grid}} \quad (2)$$

where EF_{grid} is the electricity emission factor. Using the assumed range of 0.3–0.7 kg CO_2/kWh, the indicative CO_2 reduction is ~ 1.8–6.3 kg CO_2 per tonne feed. It should be noted that the energy saving expressed per tonne of feed is primarily governed by the rejected mass fraction and does not explicitly account for the retention of TREO in the accepted stream (~57 wt% with 2.32 wt% TREO). When considering the additional energy demand of the pre-concentration step (~9.6 kWh/t under

Table 3
Mass and TREO balance summary for opto-magnetic sorting fractions (2–4 mm rauhaugite).

Fraction	Threshold setting	Mass (g)*	Mass yield (wt %)	TREO grade (wt %)	TREO recovery (%)	TREO mass in stream (g TREO per 100 g feed)**
Feed		200.0	100.0	1.71	100.0	1.71
1A (low-grade)	>160	60.8 ± 8.1	30.4	0.81 ± 0.06	14.5	0.25
1B (middle-grade)	140–160	25.2 ± 5.9	12.6	1.13 ± 0.15	8.5	0.14
1C (high-grade)	≤140	114.0 ± 13.9	57.0	2.32 ± 0.22	77.2	1.32
Sum of products		200.0	100.0		100.2	1.71
Closure		100.0%	100.0%		100.2%	100.0%

Minor deviations in the summed TREO distribution may occur due to rounding of reported mass yields and grades.
* Based on a 200 g sorting test.
** For convenience, TREO mass is also normalized to 100 g feed basis: $m_i \times G_i/m_f$ (with grade in wt%).

Table 4
ICP characterization for opto-magnetic sorting fractions (2–4 mm rauhaugite).

(ppm)	La_2O_3	Ce_2O_3	Nd_2O_3	Pr_2O_3	Y_2O_3	Dy_2O_3	Gd_2O_3	Total
Feed	4749	8291	2927	866	123	31	140	17,127
1A (low-grade)	2216	3900	1417	415	90	20	73	8132
1B (middle-grade)	3061	5470	1977	577	106	26	101	11,317
1C (high-grade)	6473	11,256	3942	1170	145	39	184	23,210

the present operating conditions), the net energy benefit is reduced and is constrained by the balance between mass rejection and TREO retention. These figures are interpreted as indicative of the potential reduction in downstream comminution demand, rather than a net energy or carbon benefit. A more rigorous assessment would require normalization to retained TREO and inclusion of process energy under pilot-scale conditions.

From a flowsheet point of view, the fractionation pattern indicates that there is a viable two-step pre-concentration process: 1A (low-grade) material can be discarded after first-pass sorting, 1C (high-grade) material can be sent for downstream processing, and the middle fraction 1B can be re-sorted or blended based on the recovery-grade compromise of the process design (Table 3). This fractionation behaviour enables a flexible flowsheet in which rejection, upgrading, and reprocessing steps can be tuned according to target recovery or grade objectives. A low-intensity magnet (0.11 T) was incorporated into the roller magnetic sorter to separate lifted particles from the magnetite powder. After magnetic lifting, the heavier mineral particles detached more readily from the magnetic field and fell into the target particle container, whereas the lighter magnetite powder remained magnetically responsive for longer, was carried further by the roller magnetic sorter, and was subsequently transferred to the upper belt magnetic separator for recovery. This density- and size-dependent detachment behaviour enables effective separation between mineral particles and magnetite powder, facilitating efficient powder recovery and reuse. Magnetite recovery remains above 99% over three consecutive reuse cycles, based on gravimetric comparison between the recovered magnetite mass and the mass added to the system.

3.2.3. *Size sensitivity (4–8 mm preliminary test)*

The 4–8 mm rauhaugite fraction was also investigated under the same operating conditions and classified into three fractions (2A, 2B, and 2C) as a preliminary size-sensitivity evaluation (Fig. 7), without separate optimization. Compared with the 4–8 mm fraction, the 2–4 mm fraction showed stronger enrichment performance. This difference is likely related to particle size effects on both sensing and actuation, including more representative surface exposure of REE-bearing phases at smaller particle sizes, which improves threshold-based optical discrimination. In addition, they show more consistent wetting behaviour and more stable magnetite-assisted lifting. In contrast, coarser particles exhibit greater variability in surface properties and lifting behaviour, which can reduce separation performance. These observations support the selection of particle size based on the trade-off between throughput and enrichment (section 2.2), and highlight the need for

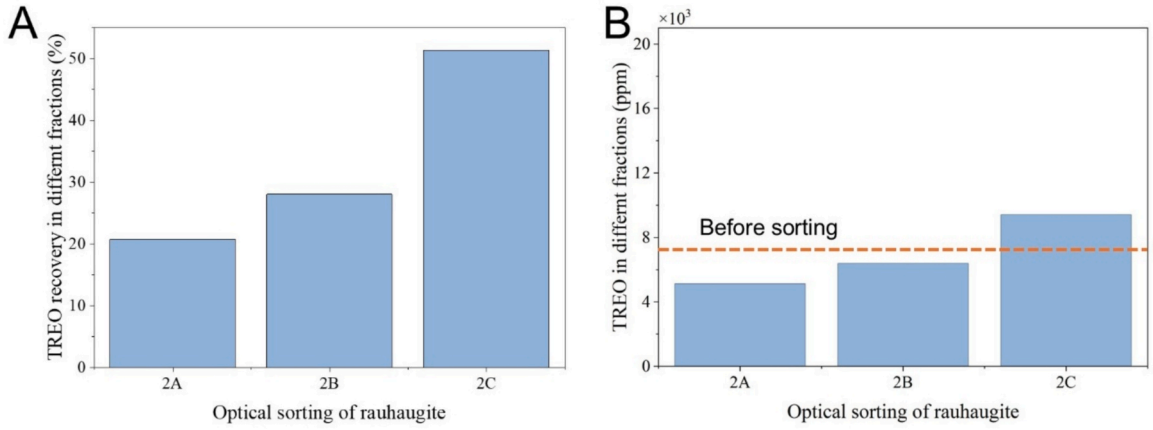

Fig. 7. Analytical results of rauhaugite (4–8 mm) after optical sorting. (A) REE recovery characterized by XRF. (B) TREO concentrations characterized by ICP-MS.

size-dependent optimization for process integration.

3.3. Applicability, limitations, and scale-up implications

Rauhaugite was used in this study to demonstrate the concept, but the selective wetting and magnetic lifting principle is not inherently specific to this ore type. Preliminary tests also indicated applicability to spodumene ores, sunflower seeds, and waste metal. Its broader application depend on identifying a suitable sensing modality to distinguish target from non-target particles among the non-ferromagnetic wettable materials. Mineral particles are washed and dried before sorting to mitigate dust- and moisture-related variability, so the present results are obtained under relatively clean and dry surface conditions. In practical operation, surface dust, residual moisture, roughness, and other surface contamination may affect droplet spreading, local wetting contrast, magnetite adhesion, and therefore lifting selectivity. Robustness under such industrially realistic surface conditions remains to be validated in future work. A low conveyor speed of 0.1 m/s is employed in this study, and this was done in order to test and validate the placement of the droplets, synchronization, and lifting selectivity. This speed is not representative of industrial speeds. Scale-up is expected to rely on lane parallelization (i.e., multiple printheads/sorting lanes), better synchronization between nozzles and belt speed, and a lifting mechanism that allows efficient recirculation of magnetite and, if needed, multiple stages of separation.

At the present stage, the method is most relevant to particle-size ranges in which localized non-pneumatic actuation provides a selectivity advantage over conventional air-based systems. In practice, the process is better suited to pre-screened narrow size fractions than to feeds with a wide particle-size distribution. This is because key process steps, including optical response, droplet deposition, wetting behavior, magnetite attachment, and magnetic lifting, are all size-dependent. Therefore, applying a single operating condition across a broad size range may reduce detection reliability and lifting selectivity. This study should be regarded as a proof-of-concept for millimeter-scale particle actuation rather than a universal solution for all ore size classes.

Magnetite recirculation adds process complexity as an extra material-handling step, although the measured recyclability of $> 99\%$ after three runs suggests that this additional loop is manageable under the current lab-scale conditions. The magnetic field strength used in this study was chosen to provide stable lifting in the current setup rather than through a systematic multi-parameter optimization. Future work should examine the combined effects of field strength, field geometry, magnetite loading, and belt speed on lifting stability and separation selectivity. Overall, the present results indicate lab-scale technical feasibility under controlled conditions, but not statistically robust validation of process performance. The optical grade relationship is ore-dependent, which may limit classification performance in ores with weak color contrast or high mineralogical variability. To improve robustness during scale-up, multimodal sensing (e.g., X-ray transmission (XRT) (Cardenas-Vera, 2022), microwave (Duan et al., 2023), and shortwave infrared) can be integrated with optical detection. Overall, the present results indicate lab-scale technical feasibility under controlled conditions, but not statistically robust validation of process performance.

4. Conclusion

To sum up, the opto-magnetic assisted sorter demonstrates the feasibility for pre-concentrating coarse REE particles on a lab scale. The prototype achieved synchronized wetting–lifting actuation and stable reject-oriented upgrading, while keeping auxiliary consumption low. For rauhaugite (2–4 mm), the process rejected a low-grade fraction corresponding to 30.4% of the feed prior to downstream processing. The high-grade fraction (57% of the feed) reached a TREO grade of 2.32% (vs. 1.71% in the feed), corresponding to an enrichment factor of ~ 1.35. Under the present lab mode, the lab system processed 84 kg/h, corresponding to approximately 1 tonne of feed processed within 12 h. Based on an instantaneous power demand of ~ 0.8 kW, this corresponds to an energy consumption of ~ 9.6 kWh/tonne under steady-state conditions. The process also exhibited low water usage ($\sim$5.7 L/tonne feed) and $>$ 99% magnetite recyclability (after 3 runs). The reported energy draw is specific to the present lab mode and should not be interpreted as projected industrial-scale performance. A simplified mass-rejection scenario suggests potential downstream comminution energy savings of $\sim$ 6–9 kWh/tonne feed. Future work should address scale-up, throughput-selectivity optimization, and validation across ores with different sensing-grade relationships.

CRediT authorship contribution statement

Hongli Su: Writing – original draft, Visualization, Validation, Methodology, Investigation, Formal analysis, Data curation, Conceptualization. **Alim Yolalmaz:** Writing – review & editing, Methodology, Investigation, Data curation. **Rajeev Bheemireddy:** Writing – review & editing, Investigation, Formal analysis, Data curation. **Yongli Wu:** Writing – review & editing, Supervision, Formal analysis. **Peter Rem:** Writing – review & editing, Methodology, Conceptualization. **Francesco Di Maio:** Writing – review & editing, Supervision, Funding acquisition, Conceptualization.

Declaration of competing interest

The authors declare that they have no known competing financial interests or personal relationships that could have appeared to influence the work reported in this paper.

Acknowledgements

This work was co-funded by the European Union under Grant Agreement No [101138353]. The views and opinions expressed are, however, those of the author(s) only and do not necessarily reflect those of the European Union or the European Health and Digital Executive Agency (HADEA). Neither the European Union nor the granting authority can be held responsible for them. The APC was funded by the TU Delft Library.

Data availability

Data will be made available on request.

References

Cuadros-Muñoz, J.-R., et al., 2024. Contribution of rare earth elements is key to the economy of the future. Land 13 (8), 1220.
Balaram, V., 2019. Rare earth elements: a review of applications, occurrence, exploration, analysis, recycling, and environmental impact. Geosci. Front. 10 (4), 1285–1303.
Opare, E.O., Struhs, E., Mirkouei, A., 2021. A comparative state-of-technology review and future directions for rare earth element separation. Renew. Sustain. Energy Rev. 143, 110917.
Zhou, B., Li, Z., Chen, C., 2017. Global potential of rare earth resources and rare earth demand from clean technologies. Minerals 7 (11), 203.
Ghorbani, Y., et al., 2025. Rare earth permanent magnets for the green energy transition: Bottlenecks, current developments and cleaner production solutions. Resour. Conserv. Recycl. 212, 107966.
Tanabe, S., 2015. Glass and rare-earth elements: a personal perspective. Int. J. Appl. Glas. Sci. 6 (4), 305–328.
Du, J., et al., 2025. Advances in rare earth catalysts for small molecule electrosynthesis☆. J. Rare Earths.
Lebrouhi, B.E., et al., 2022. Critical materials for electrical energy storage: Li-ion batteries. J. Storage Mater. 55, 105471.
Bai, Y., et al., 2024. The role of rare earths on steel and rare earth steel corrosion mechanism of research progress. Coatings 14 (4), 465.
Supriya, S., 2023. Influence of rare earth coordinated elements in titanium-based pyrochlores and their dielectric phenomena. Coord. Chem. Rev. 493, 215319.
Tan, Q., Deng, C., Li, J., 2017. Enhanced recovery of rare earth elements from waste phosphors by mechanical activation. J. Clean. Prod. 142, 2187–2191.

Zhao, T.-Y., et al., 2025. A comprehensive review on rare earth elements: resources, technologies, applications, and prospects. Rare Met. 1–30.
Norgate, T., Haque, N., 2010. Energy and greenhouse gas impacts of mining and mineral processing operations. J. Clean. Prod. 18 (3), 266–274.
Tromans, D., 2008. Mineral comminution: energy efficiency considerations. Miner. Eng. 21 (8), 613–620.
Chen, S., et al., 2020. Leaching kinetic study of sulfuric acid roasted mixed-type rare earth concentrate for reducing the solid-waste production and chemical consumption. J. Clean. Prod. 260, 120989.
Peukert, D., Xu, C., Dowd, P., 2022. A review of sensor-based sorting in mineral processing: the potential benefits of sensor fusion. Minerals 12 (11), 1364.
Sala-Garrido, R., et al., 2024. Applying the efficiency analysis tree method for enhanced eco-efficiency in municipal solid waste management: a case study of chilean municipalities. Clean Technol. 6 (4), 1565–1578.
Wübbeke, J., 2013. Rare earth elements in China: policies and narratives of reinventing an industry. Resour. Policy 38 (3), 384–394.
Nadolski, S., et al., 2018. Evaluation of bulk and particle sensor-based sorting systems for the New Afton block caving operation. Miner. Eng. 121, 169–179.
Qiu, D., Wang, C., 2019. Progress of Rare and Precious Metals Metallurgy. 2019, Metallurgical Industry Press: Beijing, China.
Modise, E.G., et al., 2022. Sensor-based ore sorting—A review of current use of electromagnetic spectrum in sorting. IEEE Access 10, 112307–112326.
Wotruba, H., Robben, C., 2020. Sensor-based ore sorting in 2020. at-Automatisierungstechnik, 2020. **68**(4): p. 231-238.
Robben, C., Wotruba, H., 2019. Sensor-based ore sorting technology in mining—past, present and future. Minerals 9 (9), 523.
Salter, J., Wyatt, N., 1991. Sorting in the minerals industry: past, present and future. Miner. Eng. 4 (7–11), 779–796.
Wijshoff, H., 2010. The dynamics of the piezo inkjet printhead operation. Phys. Rep. 491 (4–5), 77–177.
Zhang, Y., et al., 2022. Suppression and utilization of satellite droplets for inkjet printing: a review. Processes 10 (5), 932.
Tosun, A., Konak, G., 2015. Development of a model estimating energy consumption values of primary and secondary crushers. Arab. J. Geosci. 8 (2), 1133–1144.
Braeuer, F., Finck, R., McKenna, R., 2020. Comparing empirical and model-based approaches for calculating dynamic grid emission factors: an application to CO2-minimizing storage dispatch in Germany. J. Clean. Prod. 266, 121588.
Cardenas-Vera, A., et al., 2022. Investigation of Sensor-based sorting and selective comminution for pre-concentration of an unusual parisite-rich REE ore, South Namxe, Vietnam. Minerals Eng. 177, 107371.
Duan, B., Bobicki, E.R., Hum, S.V., 2023. Application of microwave imaging in sensor-based ore sorting. Miner. Eng. 202, 108303.